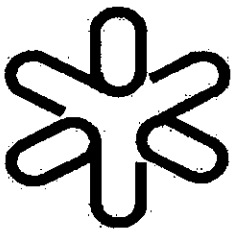

Instituto de Física
Universidade de São Paulo

Investigation of Low Energy Pion-Nucleus Interaction Using Electrofission data for Heavy Nuclei at The Pion Threshold

Deppman, A.[1] and Arruda-Neto, J.D.T.[2,3]

[1]*Laboratori Nazionali di Frascati, Instituto Nazionale di Física Nucleare*

[2]*Instituto de Física da Universidade de São Paulo, São Paulo, Brasil*

[3]*Universidade de Santo Amaro - UNISA, São Paulo (SP), Brasil*

Publicação IF - 1365/99

ABSTRACT

A theoretical approach to describe electro- and photofission processes at intermediate energies was worked out. Photopion reabsorption mechanisms by two and three nucleons ($2NA$ and $3NA$) were incorporated in the calculations. The comparison with electrofission data for preactinides showed that a substantial $3NA$ component should be added in the pion absorption to fit the data near photopion threshold, in accordance with a recent theoretical estimate. It was also shown that the shape of the fission response curve is sensitive to detailed aspects of the pion mean free path.

PACS: 25.20.Lj, 25.85.Jg

Revista :

European Journal of Physics A (IN PRESS)

1. INTRODUCTION

An increasing interest in pion-nucleus interaction has been observed in the last few years [1]. We note in this regard that, (a) the number of nucleons participating in pion absorption is one of the most intriguing questions in this field [2–4], and that (b) the pion interaction with nuclear matter, as described by its mean free path λ_π, is an open issue too, particularly for low energy pions (≤ 60 MeV) [5].

From the theoretical point of view, there are many calculations for the pion absorption probability by two, three or more nucleons inside the nucleus [6,7]. Experimentally, there are data for two and three nucleons absorption mechanisms, obtained with stopped-pions and pions with kinetic energies ≥ 60 MeV. There is, however, a large gap between ≈ 0 and ≈ 60 MeV uncovered by experimental data, as can be seen in figure 1.

In figure 2 is shown λ_π, as a function of the pion kinetic energy T_π, calculated both in the semi-classical approach [8] and in the optical model approach developed by P. Hecking [5]. The main feature of this latter result is the presence of a structure around $T_\pi \approx 40$ MeV indicating, thus, that the nuclear matter is transparent to pions with energies comprised in between ≈ 20 MeV and ≈ 60 MeV.

Recent electrofission measurements in preactinide nuclei show that pion related effects can be observed in the fission excitation curve. It was shown, in particular, that the structures in the photofission cross sections of Ta, Au and ^{182}W near the pion threshold, as derived from electrofission measurements, is related to the strong photopion reabsorption probability, similarly to the stopped-pion absorption regime [9,10]. Such (γ, f) structures reveal theirselves clearly as inflexions in the electrofission cross section curves (see discussion in references 9 and 10).

In this article we show that the shape of the inflexions systematically observed in (e, f) curves of preactinides, around $\approx 140 - 150$ MeV electron energies, is determined

by the fine characteristics of the $\lambda_\pi = \lambda_\pi(T_\pi)$ curve for $T_\pi \approx 0 - 60$ MeV. It is also shown that the magnitude of the (e,f) cross section is sensitive to the number of nucleons participating in the photopion reabsorption process allowing, thus, to determine the competition between $2NA$ and $3NA$ (two and three-nucleons absorption process, respectively). We take advantage of these two peculiarities to deduce λ_π and $2NA/3NA$ competition from ^{182}W(e,f) experimental data.

Fig. 2

The paper is organized as follows: in section 2 we discuss the relationship between $\frac{d\sigma_{e,f}}{dE}$ and $\sigma_{\gamma,f}$; in section 3 we compare the energy absorption efficiency of the different mechanisms competing in the photon absorption, and we show how this efficiency influences the photofission cross section. Section 4 is dedicated to the analysis of the electrofission cross section, and in section 5 we show the results for λ_π and $2NA/3NA$ competition obtained from the experimental data. In section 6 we present our conclusions and comments.

2. RELATIONSHIP BETWEEN INFLEXIONS IN ELECTRO AND PHOTOFISSION CROSS SECTIONS

The analysis and interpretation of the structures in the photofission cross section by means of electrofission data. require a careful search for inflexions in the electrofission yield curve.

We have shown recently [11] that for preactinides, where the photofission threshold is around 25 MeV, we have

$$\frac{d\sigma_{e,f}(E)}{dE} = \sigma_{\gamma,f}(E)\, I(E) \quad , \tag{1}$$

where $\sigma_{e,f}$ is the electrofission cross section, E is the incident electron energy, $\sigma_{\gamma,f}$ is the photofission cross section, and

$$I(E) = \frac{1}{dE}\int_E^{E+dE} N(\omega, E)d\omega \quad ; \tag{2}$$

$N(\omega, E)$ is the virtual photon density, and ω the virtual photon energy.

Since $I(E)$ is practically constant between 100 MeV and 200 MeV, it follows that

$$\frac{\frac{d\sigma_{e,f}}{dE}(E)}{\frac{d\sigma_{e,f}}{dE}(E_0)} \equiv R(E) = \frac{\sigma_{\gamma,f}(E)}{\sigma_{\gamma,f}(E_0)} \tag{3}$$

for E and E_0 (a reference energy) in that energy range (details in reference 11). We note, from eq. 3, that $\sigma_{\gamma,f}$ is directly related to the slopes of the experimentally obtained electrofission curves.

3. ENERGY ABSORPTION EFFICIENCY

The photofission cross section at intermediate energies can be expressed as [12]

$$\sigma_{\gamma,f}(E) = K\, \sigma_{\gamma,a}(E)\, \epsilon\, P_f\left(\overline{A}_{CN}, \overline{Z}_{CN}; \epsilon E\right) \quad , \tag{4}$$

where, now, E is the real photon energy, $\sigma_{\gamma,a}$ is the photoabsorption cross section, $P_f\left(\overline{A}_{CN}, \overline{Z}_{CN}; \epsilon E\right)$ is the photofission probability of the average compound nucleus $\left(\overline{A}_{CN}, \overline{Z}_{CN}\right)$, K is a phenomenological factor which is practically independent of energy (as discussed in references 12 and 13), and

$$\epsilon = \frac{\overline{E}_x}{E} \quad , \tag{5}$$

where $\overline{E}_x$ is the mean excitation energy of the compound nucleus. In fact, ϵ can be interpreted as the "nuclear efficiency for energy absorption", and it is the key quantity of our approach, as discussed below.

In figure 3, obtained from Arruda-Neto et al. [12], we show the excitation energy E_x as a function of the photon energy E. For a wide photon energy range ($E < 200$ MeV and E between 220 and 1200 MeV), E_x increases roughly linearly, indicating that ϵ is approximately constant in this range. Where ϵ is not constant, i.e., E_x is not a linear function of E, one can identify the opening of a new mechanism in the photon

absorption or a fast modification in the relative strengths of the mechanisms that are contributing to the photoabsorption process (see references 12 and 14). Fig. 3

From the discussion above, we may conclude that each photoabsorption mechanism (m) has its own efficiency ($\epsilon(m)$) in absorbing the energy of the photon, and that for a given mechanism this efficiency is approximately constant with the photon energy. It is reasonable assuming that the resulting energy absorption efficiency for the nucleus is

$$\epsilon = \sum_m \frac{\sigma^m_{\gamma,a}}{\sigma_{\gamma,a}} \epsilon(m) \quad , \tag{6}$$

where $\sigma^m_{\gamma,a}$ is the photoabsorption cross section through the mechanism m.

In the energy range of this work, the photon may be absorbed through the quasi-deuteron mechanism (QD) and/or by pion photoproduction (π). The first is a pure $2NA$ mechanism, while we assume that the π mechanism may result in pion reabsorption by a $2NA$ or a $3NA$ mechanism or, still, in the escape of the pion from the nucleus. If $P_3(E)$ is the probability of pion absorption by a $3NA$ mechanism and $P_a(T_\pi)$ is the absorption probability for pions with kinetic energy T_π, we have that

$$\frac{\sigma^{2NA}_{\gamma,a}(E)}{\sigma_{\gamma,a}(E)} = P_a(E)(1 - P_3(E)) \frac{\sigma^{\pi}_{\gamma,a}(E)}{\sigma_{\gamma,a}(E)} + \frac{\sigma^{QD}_{\gamma,a}(E)}{\sigma_{\gamma,a}(E)} \tag{7}$$

for the $2NA$ mechanism;

$$\frac{\sigma^{3NA}_{\gamma,a}(E)}{\sigma_{\gamma,a}(E)} = P_a(E)P_3(E) \frac{\sigma^{\pi}_{\gamma,a}(E)}{\sigma_{\gamma,a}(E)} \tag{8}$$

for the $3NA$ mechanism: and

$$\frac{\sigma^{esc}_{\gamma,a}(E)}{\sigma_{\gamma,a}(E)} = (1 - P_a(E)) \frac{\sigma^{\pi}_{\gamma,a}(E)}{\sigma_{\gamma,a}(E)} \tag{9}$$

for the case in which the pion escapes from the nucleus.

Then, the mean efficiency for energy absorption, $\epsilon(E)$, in this range is

$$\epsilon(E) = \left\{ P_a(E)\,(1 - P_3(E))\,\frac{\sigma^{\pi}_{\gamma,a}(E)}{\sigma_{\gamma,a}(E)} + \frac{\sigma^{QD}_{\gamma,a}(E)}{\sigma_{\gamma,a}(E)} \right\} \epsilon(2NA) + P_a(E)\,P_3(E)\frac{\sigma^{\pi}_{\gamma,a}(E)}{\sigma_{\gamma,a}(E)}\,\epsilon(3NA) \quad , \tag{10}$$

where we have neglected the low energy escaping pion contribution. We note that an escaping pion would carry away from the nucleus an energy equal to $m_\pi + T'_\pi \cong 140 + T'_\pi$ (MeV), where T'_π is the escaping pion kinetic energy; therefore, the energy left for the compound nucleus would be $\overline{E}_x \cong E - (140 + T'_\pi)$. For photons with $E \leq 180$ MeV, $\overline{E}_x \lesssim 40 - T'_\pi$; the fission cross section of preactinides at $\overline{E}_x - 40$ MeV is nearly three orders of magnitude smaller than at $\overline{E}_x \cong 180$ MeV (when the pion is absorbed), while for $E < 170$ MeV only sub-barrier fission takes place. Therefore, the fission process following the escape of a pion is negligible, in the energy range of this work, since the average excitation energy of the compound nucleus is quite low and/or smaller than the fission barrier ($\sim 25 - 30$ MeV).

Additionally, we have also neglected nucleon recoil after pion reabsorption, on the grounds of Pauli blocking arguments. As pointed out elsewhere [8], the πN phase space in the final state is reduced by the effects of the Pauli principle. As a consequence, the cross sections ratio $\sigma_{\rm qe}/\sigma_{\rm abs}$, where "qe" and "abs" stand for "quasielastic" and "absorption", respectively, decreases to *less than* 0.1 at $T_\pi = 25$ MeV. Most of the analysis performed in this work refers to T_π ranging from O to ~ 30 MeV. By assuming that at these low energies the pions keep almost unchanged their direction and energy (T_π), after undergoing quasielastic collisions, that is, $T_\pi \approx T'_\pi$, the absorption probability is given now by $P'_a = P_a(T_\pi) + P_{\rm qe}P_a(T'_\pi)$, where $P_a(T_\pi)$ and $P_a(T'_\pi)$ are the absorption probabilities without and with a quasielastic collision, respectively. Also, $P_{\rm qe} = \sigma_{\rm qe}/\sigma_{\rm reac}$ (< 0.1) and $P_a(T_\pi) \approx P_a(T'_\pi)$; thus

$P'_a \simeq P_a(T_\pi) \cdot (1 + P_{\rm qe}) < 1.1\ P_a(T_\pi)$, which is responsible for an overall uncertainty of less than 5% in the calculation of $\epsilon(E)$ (eq. 10).

It was developed by Arruda-Neto et al. [12] a formalism relating the excitation function of the compound nucleus to the energy of the nucleon initiating the intranuclear cascade (E_n) as

$$\overline{E}_x = \frac{1}{K}\,\frac{\sigma_{CN}(\overline{A}_{CN}, \overline{Z}_{CN}; E_n)}{\sigma_{\gamma,a}}\,E_n \quad , \tag{11}$$

where $\sigma_{CN}(\overline{A}_{CN}, \overline{Z}_{CN}; E_n)$ is the average compound nucleus cross section, and $\overline{A}_{CN}$ and $\overline{Z}_{CN}$ its mass and atomic number. respectively.

Deppman et al. [13] adapted this formalism for the case of the photon being absorbed by a quasi-deuteron pair. In this case, the energy of each nucleon can be considered $E_n \approx E/2$. Assuming that each nucleon will trigger an independent cascade process in the nucleus, and that the excitation energy of the compound nucleus will be the sum of the excitation energy of each cascade, from equation 11 we get

$$\overline{E}_x^{(2NA)} = \frac{1}{K}\,\frac{\sigma_{CN}(\overline{A}_{CN}, \overline{Z}_{CN}; E/2)}{\sigma_{\gamma,a}}\,E \quad . \tag{12}$$

We make here this same hypothesis for the case of three nucleons, and following the same procedure we get

$$\overline{E}_x^{(3NA)} = \frac{1}{K}\,\frac{\sigma_{CN}(\overline{A}_{CN}, \overline{Z}_{CN}; E/3)}{\sigma_{\gamma,a}}\,E \quad . \tag{13}$$

The ratio

$$\frac{\epsilon(3NA)}{\epsilon(2NA)} = \frac{\overline{E}_x^{(3NA)}}{\overline{E}_x^{(2NA)}} = \frac{\sigma_{CN}(\overline{A}_{CN}, \overline{Z}_{CN}; E/3)}{\sigma_{CN}(\overline{A}_{CN}, \overline{Z}_{CN}; E/2)} \tag{14}$$

can be calculated as shown in the Appendix.

It results that this ratio is nearly constant. and ≈ 1.5; that is, the $3NA$ mechanism is $\approx 50\%$ more efficient than the $2NA$ one. As shown below, this fact is very important in the description of the pion absorption process.

4. ANALYSIS OF THE (e,f) DATA

As discussed above, our goal is the extraction of information on pions inside the nucleus (as e. g. λ_π and $2NA/3NA$ competition) from the electrofission cross section. By using a novel technique developed at this Laboratory [11], it is possible to reconstruct the (e,f) cross section directly from the photofission cross section $\sigma_{\gamma,f}$ which, according to our approach, contains explicit informations on photopion reabsorption. These informations will appear as fitting parameters, as described below.

The quantities entering as inputs of $\sigma_{\gamma,f}$, as given by equations 4 and 10, are:

(a) $\sigma_{\gamma,a}^{QD}$, calculated by means of the well-known quasi-deuteron formalism, using parameters determined in reference 15, while for the deuteron cross section we used a parametrization given by P. Rossi et al. [16].

(b) $\sigma_{\gamma,a}^{\pi}$, obtained from the so called "universal curve" fitted by Kondratyuk et al. [17] after subtraction of the QD-component.

(c) $P_f(\overline{A}_{CN}, \overline{Z}_{CN}, \epsilon E)$, calculated through a statistical model routine using a parametrization given in reference 18, plus the fact that for preactinides $\overline{A}_{CN} = A - 1.4$ and $\overline{Z}_{CN} = Z - 0.5$. where A and Z refer to the target nucleus (see reference 18 and references therein).

(d) $\epsilon(2NA) = 0.5$ and $\epsilon(3NA) = 0.75$ because, as discussed above, $\frac{\epsilon(2NA)}{\epsilon(3NA)} = 1.5$.

The quantities considered as fitting parameters are:

(1) P_3, the $3NA$ probability. When only $2NA$ and $3NA$ mechanisms are relevant in the pion absorption process. P_3 is given by

$$P_3 = \frac{\sigma(3NA)}{\sigma(2NA) + \sigma(3NA)} \quad , \tag{15}$$

where $\sigma(2NA)$ and $\sigma(3NA)$ are the corresponding cross sections.

(2) λ_π , the pion mean free path for absorption. This quantity is introduced through the absorption probability P_a since

$$P_a = 1 - \exp\left(-\frac{R}{\lambda_\pi}\right) \quad , \tag{16}$$

where R is the nuclear radius. Also, in our approach $T_\pi \cong E - m_\pi$; thus, the function $\lambda_\pi = \lambda_\pi(T_\pi)$ converts itself into $\lambda_\pi = \lambda_\pi(E)$.

With all these inputs and fitting parameters we obtain an expression for $\epsilon(E)$ (eq. 10), which is the chief quantity for the calculation of $\sigma_{\gamma,f}$ (eq. 4). The expression for $\epsilon(E)$ takes now the form,

$$\epsilon(E) = P_a(E) \cdot B \cdot \frac{\sigma^{\pi}_{\gamma,a}}{\sigma_{\gamma,a}} + 0.5\,\frac{\sigma^{QD}_{\gamma,a}}{\sigma_{\gamma,a}} \quad , \tag{17}$$

where

$$B = 0.5 + 0.25\ P_3 \quad . \tag{18}$$

From the calculated $\sigma_{\gamma,f}$ we obtained $\frac{d\sigma_{e,f}}{dE}$ by using eq. 3 and choosing $E_0 = 100$ MeV as the reference energy; in addition, we imposed, at E_0, $\sigma_{e,f} \equiv \{\sigma_{e,f}\}_{\text{exp}}$ and $\frac{d\sigma_{e,f}}{dE} \equiv \left\{\frac{d\sigma_{e,f}}{dE}\right\}_{\text{exp}}$. The constant K appearing as a factor in eq. 4 cancels out in eq. 3. Next, we integrated numerically $\frac{d\sigma_{e,f}}{dE}$ in order to get $\sigma_{e,f}$ as a function of $\lambda_\pi(E)$ and P_3 .

5. RESULTS

The electrofission cross section of ^{182}W, recently measured at Sendai [9], is shown in figure 4.

By a mere visual inspection of eq. 17 we note that only the term $P_a(E)$ could "generate" a structure in the function $\epsilon(E)$, since $\frac{\sigma^{\pi}_{\gamma,a}}{\sigma_{\gamma,a}}$ and $\frac{\sigma^{QD}_{\gamma,a}}{\sigma_{\gamma,a}}$ are monotonic functions of E . On the other hand, structures in $\epsilon(E)$ manifest theirselves as structures and

inflexions in $\sigma_{\gamma,f}$ (figure 5) and $\sigma_{e,f}$ (figure 4), respectively. The only role played by the term B is that of displacing the curves up or down.

The starting point of our analysis was the attempt to reproduce the inflexion observed in the ^{182}W(e,f) data around 140 – 160 MeV (figure 4) assuming, for the sake of simplicity, that $P_3 = 0$ (i.e., B=0.5). The results correspond to curves **1** in figure $4(a,b,c)$, for three choices of the function $\lambda_\pi = \lambda_\pi(E)$ or, in other words, for three distinct choices of pion absorption probabilities P_a (equation 16).

For the calculation of curve **1**, in figure 4a, we used a $\lambda_\pi(E)$ obtained from the figure 5.2 of reference 8 – also shown in our figure 2-curve **a**, while for curve **1** in figure 4b we used a theoretical calculation of $\lambda_\pi(E)$ performed by Hecking [5] which corresponds to λ_π-absorption (fig. 1 in reference 5: curve-II-dashed, $\rho = \rho_0$); see our figure 2 – curve **b**. As we can see, the $\lambda_\pi(E)$ from reference 8 is inadequate, while that from reference 5, although providing better agreement in terms of magnitude, could not reproduce the (e,f) inflexion. We observed by means of simulation that the shape of the function $\lambda_\pi = \lambda_\pi(E)$, calculated by Hecking [5], is reasonable but its magnitude is not. In fact, by increasing the magnitude (and keeping the shape fixed) we were able in reproducing quite well the observed (e,f) inflexion (curve **1** in figure 4c).

Fig. 4

It is quite instructive to note that the higher is the $\lambda_\pi(E)$ magnitude the more pronounced is the (e,f) inflexion, but this process causes a lowering of the (e,f) cross section magnitude.

In order to fit the magnitude of the data points it was necessary to add the term $0.25\,P_3$ to B (eq. 18). The best fit was obtained for $P_3 \cong 0.35$ (curve **2** in figure 4c).

Uncertainties arising from the ingredients of eq. 10 are greatly reduced, since we take ratios of the calculated (γ,f) cross section to obtain $\sigma_{e,f}$ (eq. 3). The overall uncertainties of curves **1** and **2** (figure 4) are better than $\approx 15\%$ in their relative magnitudes.

We note, additionally, that for $E \lesssim 140$ MeV where only the QD-mechanism plays a role, the (γ, f) cross section takes the form (see eqs. 4 and 17)

$$\sigma_{\gamma,f}(E) = 0.5\ K\ \sigma^{QD}_{\gamma,a}(E)\ P_f\left(\overline{A}_{CN}, \overline{Z}_{CN}; 0.5\ E\right) \tag{19}$$

since, now, $\sigma_{\gamma,a} = \sigma^{QD}_{\gamma,a}$. We used this expression for the calculation of $\sigma_{e,f}$ in the energy range 100 – 140 MeV obtaining, thus, an excellent agreement with the (e, f) data (figure 4). This is a good evidence to the fact that the inputs used in our calculations are reasonable.

6. CONCLUSIONS AND FINAL REMARKS

Finally, we can drawn the following conclusions:

(1) the probability for the $3NA$ process is $P_3 \cong 0.35$, provided the pion mean free path be that shown in figure 2 - curve **c**, which was able in reproducing the inflexion observed in the (e, f) experimental curve of ^{182}W;

(2) our finding that $P_3 \cong 0.35$ agrees well with a calculation performed by Simicevic [7] in the range $T_\pi \cong 0$ – 40 MeV. Quite recently, moreover, H. Hahn and collaborators [19] measured positive and negative pion absorption on ^3He at $T_\pi = 37$ MeV; it was found that the probabilities for $3NA$ are 0.14 ± 0.04 and 0.65 ± 0.12, respectively – the average is 0.39 ± 0.13. which also is in good agreement with our finding;

(3) the inflexion exhibited by the experimental (e,f) curve of ^{182}W, (and other preactinides), around 140 MeV. strongly suggests that the nuclear matter is transparent to low energy pions, with a mean free path given by curve **c** of figure 2, since only in this case an inflexion is obtained in the calculated curves (fig. 4-c). This is in qualitative agreement with the calculation of Hecking (curve **b** in figure 2). We refer the reader to reference 5 for more details on the issue of nuclear transparency to pions.

(4) in figure 5 we plotted the photofission cross section as a function of the photon energy, according to our model. The solid line was calculated by using $P_3 = 0.35$ and the pion mean free path given by curve **c** of figure 2. The dashed curve was obtained by assuming that there is no $3NA$ mechanism, and using Hecking's mean free path (curve **b** in figure 2). The fast increasing of the solid curve is due to the presence of $3NA$ pion reabsorption. This mechanism is more efficient in absorbing the photon energy and leads the compound nucleus to a higher excitation energy, comparatively with the $2NA$ mechanism. Since the fission probability is an increasing function of the excitation energy, this results in a higher fission probability for compound nuclei following $3NA$. The valley between 150 – 175 MeV is more pronounced in the solid line because the pion mean free path is higher in this energy range (see figure 2).

Fig. 5

We mention, as final remarks, that the photonuclear process is quite effective to probe the behavior of pions inside the dense portion of the nuclear matter, while in pion scattering mostly the nuclear surface is probed. In fact, Oset [20] pointed out recently that the magnitude of the indirect photoabsorption cross section, σ_{ind} (which corresponds to photoabsorption where the pions are absorbed), can provide more information about the pion absorption probability than the pion absorption cross section obtained from the scattering of real pions on nuclei. In this regard we can say that, being the shape of the electrofission curve very dependent on λ_π, this cross section reflects the magnitude of σ_{ind} and, therefore, allows us to access the absorption of low- energy pion in heavy nuclei, as demonstrated in this work.

APPENDIX

The $3NA$ excitation energy of the compound nucleus

The compound nucleus excitation energy, $\overline{E}_x$, is given by [13]

$$E_x = \left(\sum_{S=S_c}^{\infty} (1 - \gamma S_\infty) \sigma^{(S)} \left(E_0 - \overline{E}_F \right) + \sum_{S=S_c}^{\infty} \sum_{k=1}^{S-S_c} \gamma^k \sigma^{(S)} \left(E_0 - \overline{E}_F \right) \right) \frac{(E_0 - \overline{E}_F)}{\sigma_{\gamma,a}(E)} \tag{A.1}$$

where γ is a constant depending only on the nuclear structure, $\frac{\sigma^{(S)}}{\sigma_{\gamma,a}}$ is the probability that a nucleon with initial energy E_0 will trigger a cascade with S steps (see [13] and references therein), $S_\infty = \frac{1}{1-\gamma}$, $\overline{E}_F$ is the average Fermi-energy of the nucleons in the target nucleus.

The initial energy E_0 is given, for the $3NA$ process, by

$$E_0 = \frac{E}{3} + \overline{E}_F \quad , \tag{A.2}$$

and assuming that each of the three nucleons will trigger an independent cascade process, the resulting compound nucleus excitation energy will be the sum of the excitation energy contributions from each cascade:

$$\overline{E}_x = 3 \left(\sum_{S=S_c}^{\infty} (1 - \gamma S_\infty) \sigma^{(S)}(E/3) + \sum_{S=S_c}^{\infty} \sum_{K=1}^{S-S_c} \gamma^k \, \sigma^{(S)}(E/3) \right) \frac{\frac{E}{3}}{\sigma_{\gamma,a}(E)} \quad ; \tag{A.3}$$

defining, as done in [13], k so that

$$\frac{\sigma_{CN}(E)}{K} = \sum_{S=S_c}^{\infty} (1 - \gamma \, S_\infty) \sigma^{(S)}(E) + \sum_{S=S_c}^{S-S_c} \gamma^k \, \sigma^{(S)}(E) \quad , \tag{A.4}$$

where

$$\sigma_{CN}(E) = \sum_{S=S_c}^{\infty} \sigma^{(S)} \quad , \tag{A.5}$$

we get

$$\sigma_{CN}(E/3) = K(E/3) \frac{\overline{E}_x}{E} \sigma_{\gamma,a}(E) \quad . \tag{A.6}$$

Since $K(E)$ is approximately independent of the energy [13], we can write

$$\sigma_{CN}(E/3) = K\frac{\overline{E}_x}{E}\sigma_{\gamma,a}(E) \quad , \tag{A.7}$$

and then,

$$\epsilon(3NA) = \frac{\overline{E}_x}{E} = \frac{1}{K}\,\frac{\sigma_{CN}(E/3)}{\sigma_{\gamma,a}(E)} \quad . \tag{A.8}$$

For the $2NA$ process, and for the same reasons, we get

$$\epsilon(2NA) = \frac{\overline{E}_x}{E} = \frac{1}{K}\,\frac{\sigma_{CN}(E/2)}{\sigma_{\gamma,a}(E)} \quad . \tag{A.9}$$

So,

$$\frac{\epsilon(3NA)}{\epsilon(2NA)} = \frac{\sigma_{CN}(E/3)}{\sigma_{CN}(E/2)} \quad . \tag{A.10}$$

This ratio can be calculated by using eq. (A.5), once it depends only on the nucleon's mean free path inside the nucleus.

REFERENCES

1. Weyer, H.J.: *Phys. Reports* **195**, 295 (1990).
2. Steinacker, M. et al.: *Nucl. Phys.* **A517**, 413 (1990).
3. Laget, J.M.: *Nucl. Phys.* **A579**, 333 (1994).
4. Backenstoss, G. et al.: Paul Scherrer Institute, PR-95–27 (1995).
5. Hecking, P.: *Phys. Lett.* **B103**, 401 (1981).
6. Oset, E., Futami, Y., and Toki, H.: *Nucl. Phys.* **A448**, 597 (1986).
7. Simicevic, N.: *Phys. Rev.* **C50**, 2224 (1994).
8. Ericson, T., and Weise, W.: *Pions and Nuclei*, Oxford Science Publications 1988.
9. Arruda-Neto, J.D.T. et al.: *Phys. Rev.* **C48**, 1594 (1993).
10. Arruda-Neto, J.D.T. et al.: *Phys. Rev.* **C51**, 452 (1995).
11. Deppman, A., Arruda-Neto, J.D.T., and Tavares, M.V.: *Nucl. Instr. Meth.* **A384**, 516 (1997).
12. Arruda-Neto, J.D.T. et al.: *Phys. Rev.* **C51**, 751 (1995).
13. Deppman, A. et al.: *Il Nuovo Cim.* **109A**, 1197 (1996).
14. Arruda-Neto, J.D.T. et al.: *Phys. Rev.* **C54**, 3294, 1996.
15. Tavares, O.A.P., and Terranova, M.L.: *J. Phys.* **G18**, 521 (1992).
16. Rossi, P. et al.: *Phys. Rev.* **C40**, 2412 (1989).
17. Kondratyuk, L. et al.: *Nucl. Phys.* **A579**, 453 (1994).
18. Guaraldo, C. et al.: *Il Nuovo Cim.*. **103A**, 607 (1990).
19. Hahn, H. et al.: *Phys. Rev.* **C53**, 1074 (1996).
20. Oset, E.: Proc. V La Rábida Int. Summer School on *Nucl. Phys.* , Huelva, Spain, Springer 1994.

FIGURE CAPTIONS

Figure 1: Contribution of the $3NA$ mechanism to the total pion absorption as a function of pion kinetic energy. The curves are calculations by Simicevic [7] (continuous line) and by Oset et al. [6] (dashed line). The full squares are the experimental results for ^3He, from ref. 1 (fig. 24, page 350); the open square is the recent result for ^3He obtained in ref. 19 (see text). The full circles are experimental results for pion absorption on complex nuclei leading to three protons in the final state, extracted from ref. 1 (fig. 22, page 348), multiplied by a factor 4 (error bars are not shown).

Figure 2: Pion mean free path in nuclear matter as a function of the kinetic energy. The curve **a** is taken from ref. 8; curve **b** is calculated in ref. 5; and curve **c** is the best curve we found to fit the (e, f) data (see text).

Figure 3: Mean excitation energy as a function of the photon energy, adapted from ref. 12.

Figure 4: Electrofission cross section of ^{182}W as a function of the incident electron energy. Data are from ref. 10. The curves are the result of our calculation assuming only a $2NA$ mechanism for pion absorption (labeled **1**), or considering contributions from both $2NA$ and $3NA$ (labeled **2**) as discussed in the text. In figure a) we used the semi-classical λ_π from ref. 8 (curve **a** in fig. 2); the Hecking calculation [5] (curve **b** in fig. 2) was used for λ_π in figure b); and in figure c) is the calculation using λ_π as described by curve **c** in fig. 2, which provided the best fit to the (e, f) data.

Figure 5: ^{182}W photofission cross section calculated according to our model. The solid line is obtained considering a $3NA$ contribution equivalent to $P_3 = 0.35$, and the pion mean free path given by curve **c** in figure 2. The dashed line is calculated assuming that there is no $3NA$ contribution, and using the pion mean free path from ref. 5.

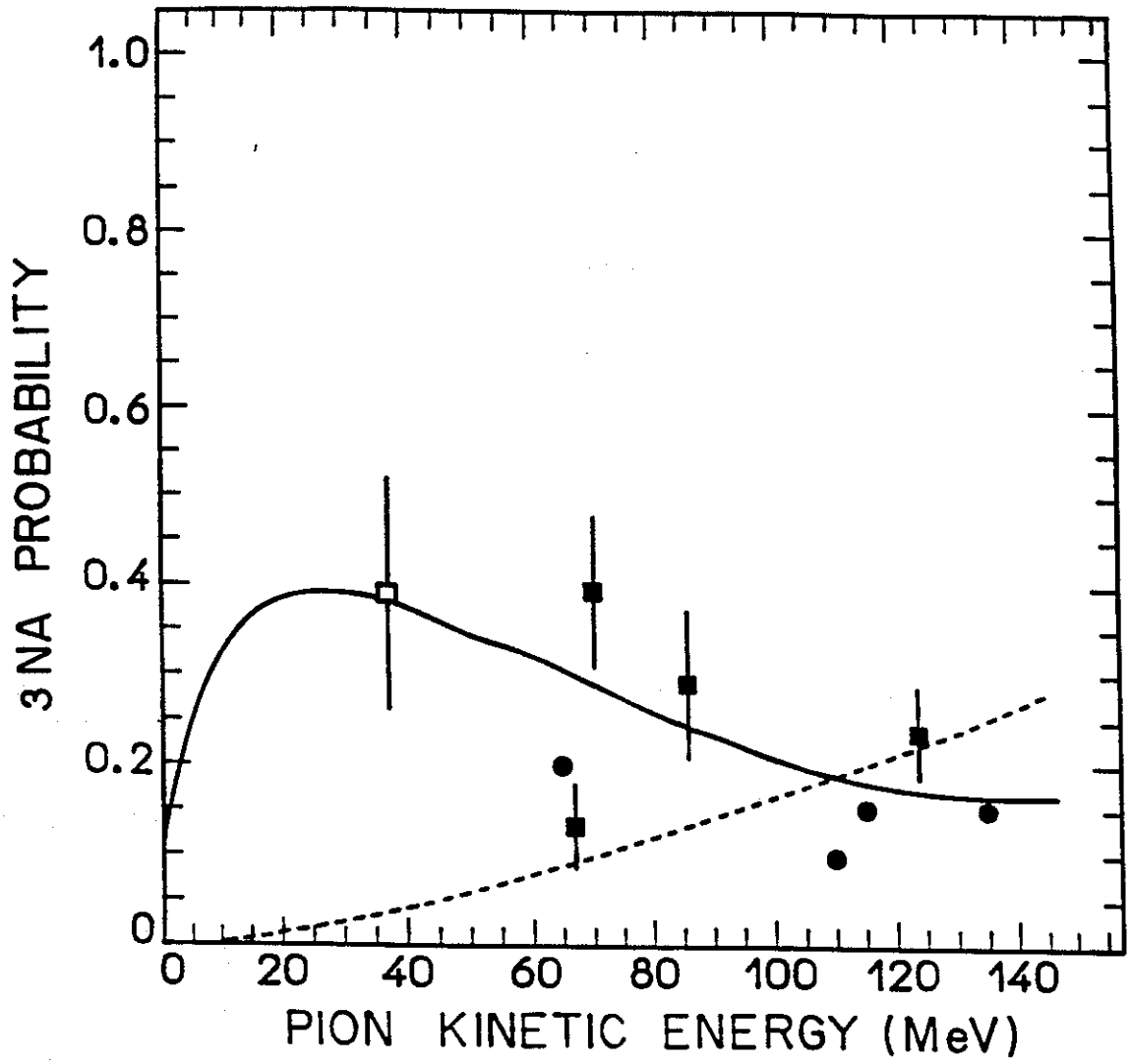
1.0
0.8
0.6
0.4
0.2
0
3NA PROBABILITY
0
20
40
60
80
100
120
140
PION KINETIC ENERGY (MeV)

Fig. 1

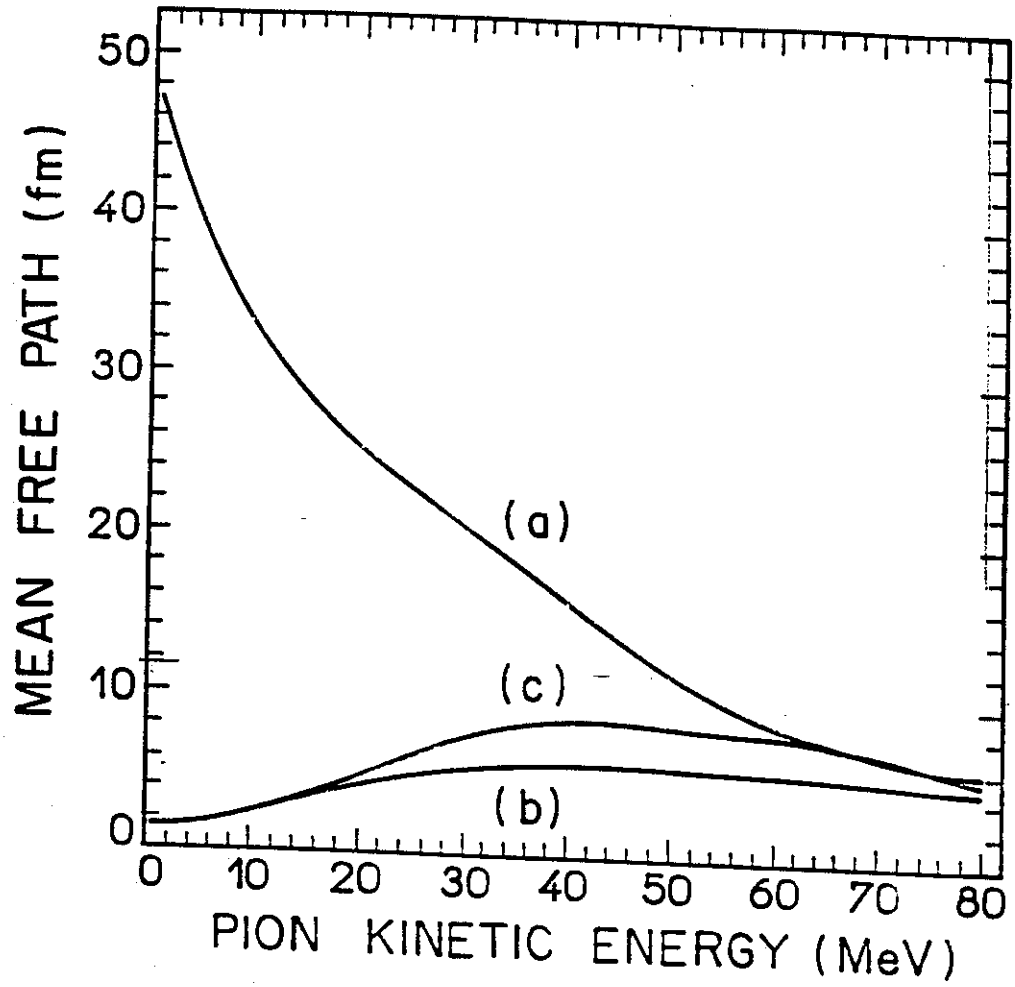
MEAN FREE PATH (fm)
50
40
30
20
10
0
(a)
(c)
(b)
0
10
20
30
40
50
60
70
80
PION KINETIC ENERGY (MeV)

Fig. 2

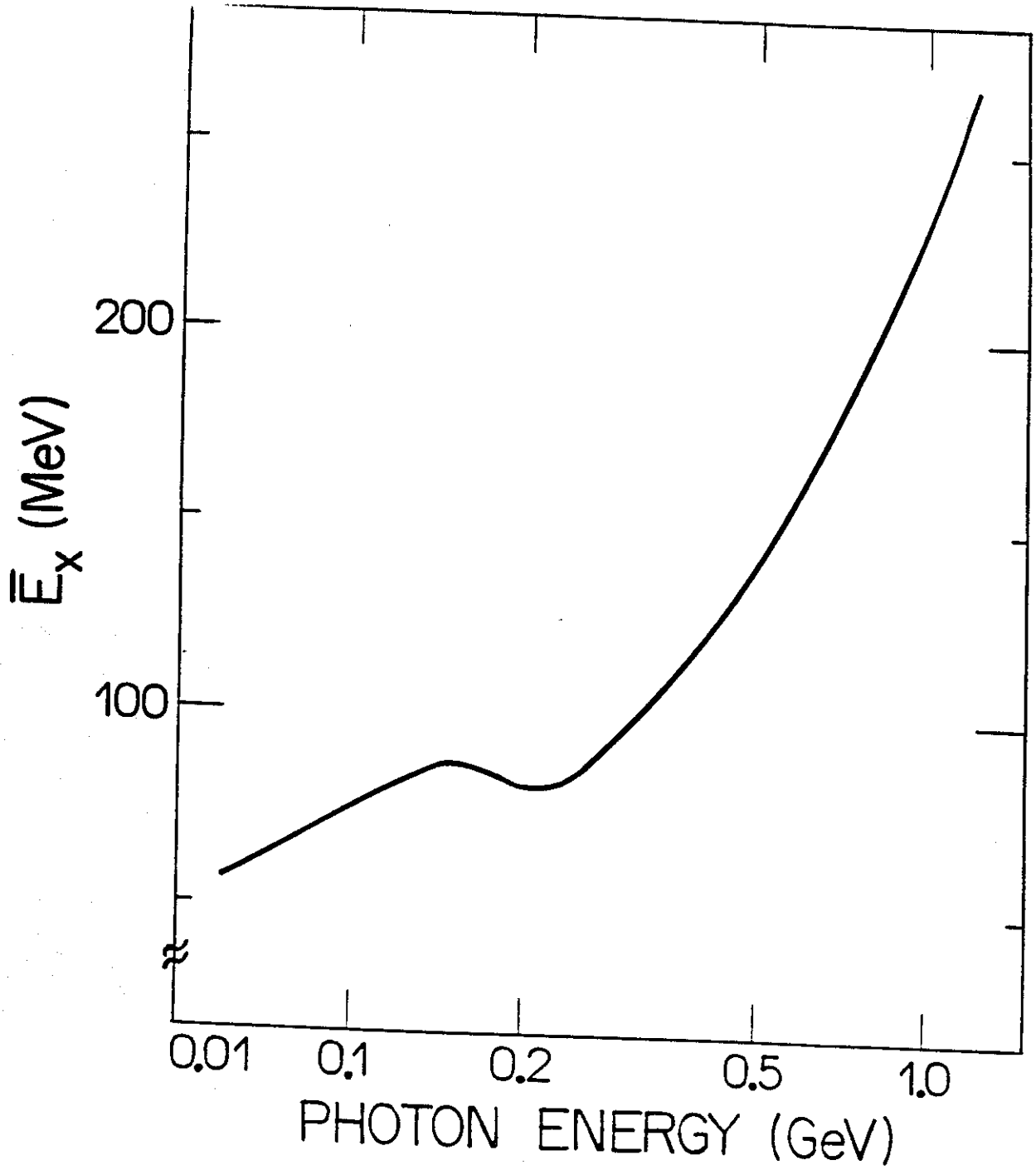

Fig. 3

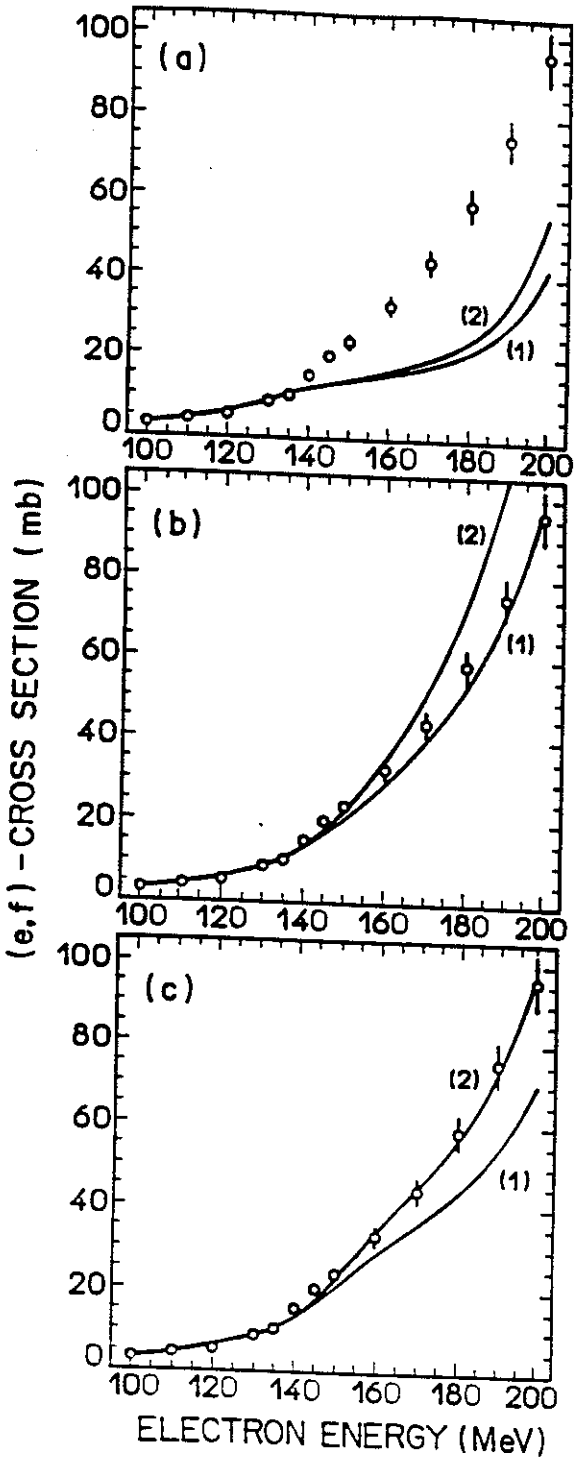
(a)
(b)
(c)
(1)
(2)
(e,f) - CROSS SECTION (mb)
ELECTRON ENERGY (MeV)
0
20
40
60
80
100
100 120 140 160 180 200

Fig. 4

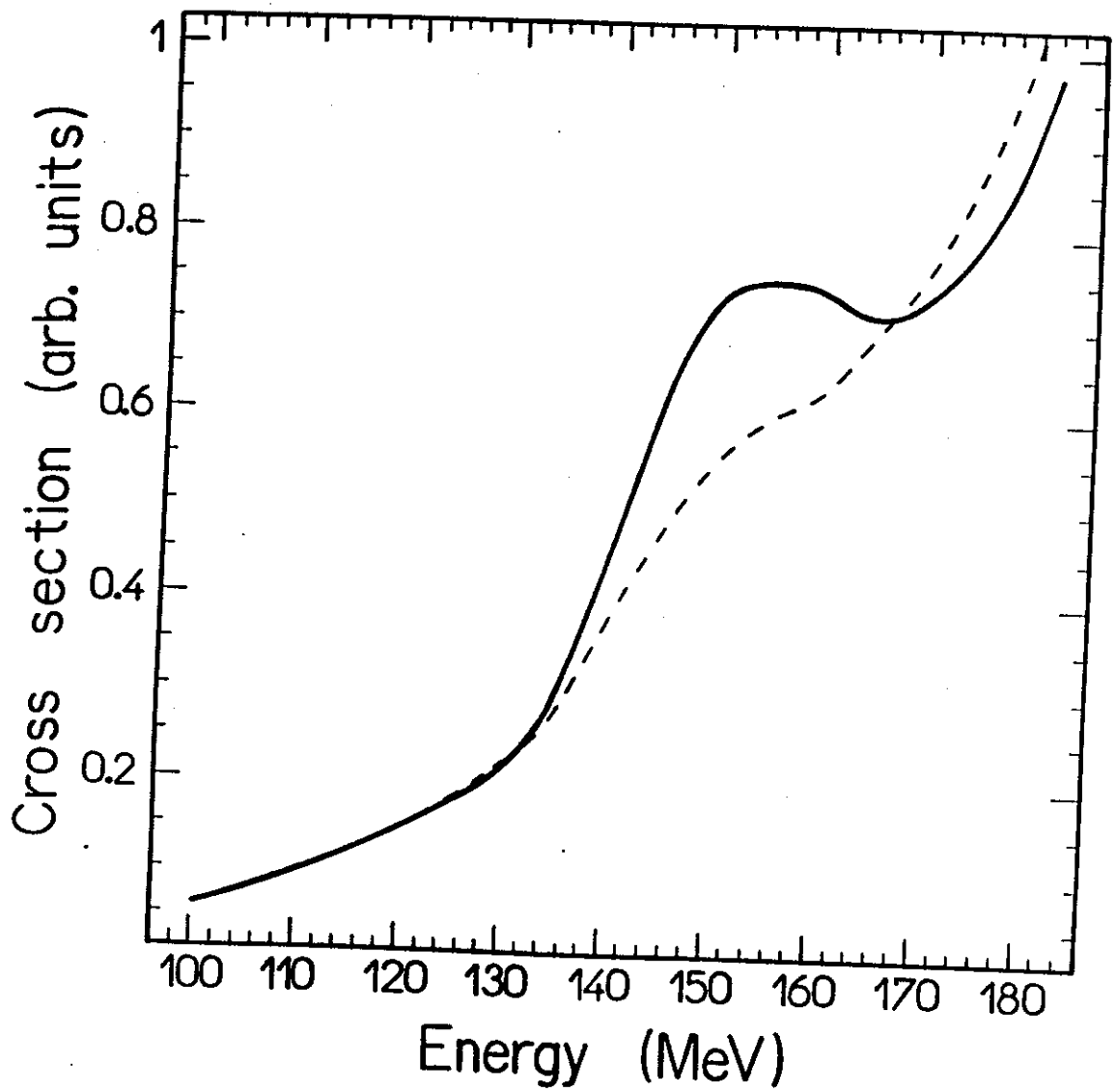
Cross section (arb. units)
1
0.8
0.6
0.4
0.2
100
110
120
130
140
150
160
170
180
Energy (MeV)

Fig. 5